BIOCHEMISTRY
including biophysical chemistry & molecular biology
Article

Biochemistry **2010,** *49,* 893–904 893
DOI: 10.1021/bi901282s

Recognition by the Thyroid Hormone Receptor of Canonical DNA Response Elements†

Ana Carolina Migliorini Figueira,[‡,||] Luís Maurício T. R. Lima,[§,||] Leonardo H. F. Lima,[‡] Americo T. Ranzani,[‡] Guilherme dos Santos Mule,[§] and Igor Polikarpov*,[‡]

[‡]*Instituto de Física de São Carlos, Universidade de São Paulo, Av. Trabalhador Sãocarlense, 400, São Carlos, SP, Brazil 13560-970 and* [§]*Faculdade de Farmácia, Universidade Federal do Rio de Janeiro, Ilha do Fundão, Rio de Janeiro, RJ, Brazil 21941-590.* [||]*These authors contributed equally to this work.*

Received July 26, 2009; Revised Manuscript Received December 20, 2009

ABSTRACT: To shed more light on the molecular requirements for recognition of thyroid response elements (TREs) by thyroid receptors (TRs), we compared the specific aspects of DNA TRE recognition by different TR constructs. Using fluorescence anisotropy, we performed a detailed and hierarchical study of TR−TRE binding. This was done by comparing the binding affinities of three different TR constructs for four different TRE DNA elements, including palindromic sequences and direct repeats (F2, PAL, DR-1, and DR-4) as well as their interactions with nonspecific DNA sequences. The effect of $MgCl_2$ on suppressing of nonselective DNA binding to TR was also investigated. Furthermore, we determined the dissociation constants of the hTRβ DBD (DNA binding domain) and hTRβ DBD-LBD (DNA binding and ligand binding domains) for specific TREs. We found that a minimum DNA recognition peptide derived from DBD (H1TR) is sufficient for recognition and interaction with TREs, whereas scrambled DNA sequences were unrecognized. Additionally, we determined that the TR DBD binds to F2, PAL, and DR-4 with high affinity and similar K_d values. The TR DBD-LBD recognizes all the tested TREs but binds preferentially to F2, with even higher affinity. Finally, our results demonstrate the important role played by LBDs in modulating TR−DNA binding.

The thyroid hormone receptors (TRs)[1] are ligand-modulated transcription factors that belong to a large nuclear receptor superfamily, including retinoic X receptor (RXR) and steroid and vitamin D receptors (*1*, *2*). Members of this gene family activate transcription by binding to specific DNA sequences, termed hormone response elements (HREs), which are generally located in the vicinity of target genes (*3*). The TRs are multidomain proteins that contain a poorly conserved N-terminal domain, a central strongly conserved DNA binding domain (DBD), and a C-terminal ligand binding domain (LBD). The DBD contains two highly conserved zinc finger structural motifs, responsible for DNA binding, each of which possesses four cysteine residues coordinating with one zinc atom (*3*, *4*). The carboxy terminus of the first zinc finger contains a P-box region that determines DNA sequence specificity. Furthermore, a short loop between the first and second zinc finger (D-box) forms a dimerization interface with the DBDs, which determines the spacing between DNA binding half-sites (*5*, *6*). The C-terminal half of the receptor encompasses the ligand binding domain (LBD), which has an essential role in hormone recognition, in coregulator recruitment, and in inducing physiological response specificity. The LBD can be considered a molecular switch that is activated upon ligand binding to induce gene transcription (*7*).

Thyroid receptors can act as both transcriptional repressors and activators. These dual functions are dependent on the interactions with its cognate hormones (3,5,3′-triiodothyronine, T3, and thyroxine, T4). The thyroid hormones (T3 and T4) regulate a wide range of physiological processes, such as differentiation, development, growth, and metabolism in mammals as well as other organisms (*8*−*10*). In the absence of ligand, the TRs strongly repress transcription from some promoters to which they bind (*11*). This type of regulation also exists in the chicken lysozyme silencer element, growth hormone promoter, malic enzyme and thyroid stimulating hormone (TSH) promoters, among others (*12*, *13*). TR recruits corepressors, which can also activate rather than suppress basal transcription of genes negatively regulated by the thyroid hormone. When the TR is exposed to an agonist, these repressive effects are relieved and transcription is initiated through coactivator recruitment. These variations provide a wide range of transcriptional activity levels (*14*).

The effects of the TR on gene regulation occur after its binding to specific DNA sequences in the regulatory regions of the target genes (*12*). These regions, known as thyroid response elements (TREs), normally contain at least two half-sites composed of hexameric nucleotide sequences derived from an AGGTCA consensus sequence (*1*, *12*). These half-sites can have different arrangements, and their arrays and orientations determine the differences in ligand binding (*15*). The most common TREs can be arranged as (i) direct repeats separated by four nucleotides (DR-4) (*1*, *15*, *16*), (ii) inverted palindromes separated by six nucleotides (IP-6 or F2), and (iii) response elements consisting of

†This work was supported by the Conselho Nacional de Desenvolvimento Científico e Tecnológico (CNPq) (to L.M.T.R.L. and I.P.) and by Fundação de Amparo à Pesquisa do Estado de São Paulo (FAPESP) Grants 03/09462-5, 2006/00182-8, 2007/01441-0, and 2008/00078-1 to I.P.

*To whom correspondence should be addressed. Phone: +55(16) 3373-9874. Fax: +55(16) 3373-9881. E-mail: ipolikarpov@ifsc.usp.br.

[1]Abbreviations: TR, thyroid receptor; HRE, hormone response element; TRE, thyroid hormone response element; F2, inverted palindrome separated by 6 bp; PAL, palindrome with no separation; DR-1, direct repetition separated by 1 bp; DR-4, direct repetition spaced by 4 bp; DBD, DNA binding domain; LBD, ligand binding domain; T3, triiodothyronine; RXR, retinoic X receptor.

Published on Web 12/21/2009

two hexamers in a palindrome arrangement with no spacer (PAL). This latter arrangement is similar to those described for estrogen, progesterone, and glucocorticoid receptors (*1*, *17*, *18*). The relative orientation and spacing of the recognition motifs play essential roles in the specificity of binding of the TR to TRE DNA and transcriptional activation. The palindromic TREs are considered prime response elements to TR (*19*). In contrast, the direct repeats spaced by 4 bp display preferential binding and activation responses compared to those of the TR−RXR heterodimer (*6*). Additionally, the spacer sequence, present between the two half-sites, also can influence the binding and affinity between NRs and HREs (*15*).

In the absence of ligand, the TRs bind to DNA as monomers and homodimers (*20*). It is generally accepted that to exert their function the TR homodimers bind with high affinity to DNA sequences arranged as inverted palindromes (IPs). Transactivation assays have shown that TR−TRE binding and transcription activation have the following order of preference: F2 (or IP-6) > IP-4 > PAL > IP-9 > DR-4 (*13*). TR is also capable of heterodimerizaion with RXR in the presence of T3 (*21*−*24*). T3 destabilizes the binding of TR homodimers to a subset of TREs (*25*), promoting dissociation of the dimer into monomers, and, consequently, enables the heterodimerization event (*13*, *25*). Therefore, T3, at physiologic concentrations, modifies the balance between homo- and heterodimers bound to DNA (*17*). TR homodimers bind with a high affinity to everted palindromic elements, which contain the half-site motifs separated by 4, 5, or 6 bp. A strong cooperative effect is observed between TR homodimers and inverse palindromes (F2), but not with direct repeat response elements (as DR-4) (*26*). This cooperative binding is similar to that observed for TR−RXR heterodimer interaction with all TREs (*13*). However, the binding constants and the hierarchic contribution of different TR domains in modulating recognition by diverse TREs still require clarification. We provide here a quantitative and hierarchical characterization of the binding affinities among three different TR constructs and four specific TREs (F2, PAL, DR-4, and DR-1) as well as irrelevant DNA sequences. The TR constructs were the isolated TR DBD recognition helix (H1TR), the complete TR DNA binding domain (DBD), and the TR DBD attached to the ligand binding domain (TR DBD-LBD).

EXPERIMENTAL PROCEDURES

Protein Expression and Purification. The full-length nuclear receptors are notoriously difficult to express and purify. Therefore, we conducted our studies using the human TR DBD (amino acid residues 102−198) and the human TR DBD-LBD constructs (residues 102−461). It is important to mention that bacterially expressed TR DBD-LBD fully recapitulates the DNA binding and oligomerization properties of full-length TR (*26*−*28*). The constructs were fused in frame to the C-terminus of a polyhistidine (His) tag and were expressed in *Escherichia coli* strain BL21(DE3) harboring a pET28a(+) plasmid (Novagen). The modified expression and purification protocols were applied (*26*).

The labeled TR LBD-DBD containing a fluorescein molecule was prepared by incubation of the TR and the probe, fluorescein isothiocyanate, in a 3-fold molar excess, for 2 h at 10 °C. The protein−probe complex was applied to a HiTrap desalting column (GE Healthcare), to separate excess fluorescein from the TR−fluorescein complex.

The 14-amino acid peptide corresponding to the DNA recognition helix of TR (H1TR), with sequence H_2N-CEGCK-GFFRRTIQK-COOH, was synthesized and HPLC-purified by Genemed. The molecular weights of all the proteins were confirmed by mass spectrometry, and their DNA sequences were identified by nucleotide sequencing.

We also confirmed the fraction of the active protein in our preparations by three different techniques: gel shift mobility assay with DNA responsive elements, anisotropy assay of DNA binding under stoichiometric conditions, and independent small-angle X-ray scattering studies (SAXS) (*28*).

Synthetic Oligonucleotides. The single-stranded synthetic oligonucleotides, high-pressure liquid chromatography-purified and with fluorescein attached at the 5′ sense single-stranded end, were purchased from Alpha DNA. The double-stranded 18−26 bp oligonucleotides containing two TR motifs (A/GGGTCA) were as follows: IP-6 or F2, 5′ AGCTTA-TTGACCCCAGCTGAGGTCAAGTTACG 3′; PAL, 5′ ATATTCAGGTCATGACCTGAATAT 3′; DR-4, 5′ AGCTA-AAGGTCAGATCAGGTCAGTAGGA 3′; DR-1, 5′ AGCTA-AAGGTCAGAGGTCAGTAGGA 3′; p53 consensus DNA, 5′ TAATTAGGCATGTCTAGGAAA 3′; recA consensus DNA, 5′ ACTGTATGAGCATACAGTA 3′; and E2 consensus DNA, 5′ GTAACCGAAATCGGTTGA 3′. They (recognition half-sequences, when they appear, are underlined) were paired with their complementary strand and annealed in a PCR apparatus (Perkin-Elmer 480 programmable thermocycler) at equimolar concentrations in water. The pairing procedure included heating at 100 °C for 10 min and slow cooling to 25 °C.

Nondenaturant Polyacrylamide Gel Electrophoresis. To assess TR−DNA binding, 48 μM hTRβ1 DBD-LBD (expressed as monomers) was incubated for 2 h at 4 °C in 20 mM Hepes (pH 8.0), 50 mM NaCl, 5% glycerol, and 3 mM DTT with 24 μM TREs (F2, PAL, DR-1, and DR-4), subjected to an 8 to 25% (w/v), pH 8.8 gradient polyacrylamide gel using the Phast System (GE Healthcare), at 4 °C, and Coomassie blue, and stained with ethidium bromide. The mobility of the individual protein standards [thyroglobulin (667 kDa), ferritin (440 kDa), catalase (232 kDa), aldolase (132 kDa), and albumin (67 kDa)] was plotted as the retardation factor (R_f) versus the hydrodynamic radius (R_h). The linear equation obtained from this calibration was employed to calculate the R_h of the fractions of hTRβ1 DBD-LBD tetramers (without the TREs) and the complexes of hTRβ1 DBD-LBD dimers bound to DNA (*29*).

Fluorescence Anisotropy. An anisotropy binding titration assay with the H1TR peptide was performed in a Jasco FP-6300 spectrofluorimeter. Anisotropy measurements were conducted in "L" geometry. Excitation was set to 480 nm and emission at 520 nm, recorded through Glan-Thompson polarizers. Anisotropy values (R) were calculated according to the equation (*30*)

$$R = (I_{VV} - GI_{VH})/(I_{VV} + 2GI_{VH}) \quad (1)$$

where I refers to the measured fluorescence intensity, indices V (vertical) and H (horizontal) are the positions of the polarizers at excitation (first index) and emission (second index), and G is a correction factor, which takes into account differences in sensitivity in the two directions, I_{VV} and I_{VH}, according to

$$G = I_{HV}/I_{HH} \quad (2)$$

Anisotropy measurements with the recombinant TR constructs were performed in an ISS-PC1 spectrofluorimeter (ISS, Champaign,

IL), assembled in L geometry. Excitation was set to 480 nm, and emission was recorded through an OG515 orange short-wave cutoff filter (cutoff, 50% at 515 nm). Anisotropy values were calculated with the ISS program, according to eq 1. Data were corrected for fractional contributions by fluorescence over anisotropy. All fluorescence anisotropy data shown in this study are an average of at least three independent experiments, performed with different protein batches and on different days. For each sample, anisotropy was measured until the absolute errors were less than 0.002.

Titrimetric Assay of the TR−TR Interaction. To analyze the oligomeric state of apo-TR DBD-LBD (i.e., TR without T3), in the absence of the TREs, we performed an anisotropy binding titration assay by incubating 5 nM fluorescein-labeled TR DBD-LBD with unlabeled apo-TR DBD-LBD at concentrations ranging from 10 nM to 10 μM (concentrations expressed as TR monomers). The assay was performed at 10 °C in 50 mM NaCl, 20 mM Hepes (pH 8.0), 3 mM dithiothreitol, and 5% glycerol. TR−TR binding assays were analyzed assuming a simple two-state reversible equilibrium between TRs as described previously (*31*).

The oligomeric state of TR at each protein preparation (apo-TR) was confirmed by chemical cross-linking (data not shown). The apoproteins, at 0.5 and 5 μM, were cross-linked by exposure to 5 μM suberic acid bis-*N*-hydroxysuccinimide ester (DSS) (Sigma) (*27*). Samples were subjected to SDS−PAGE and further silver stained.

Titrimetric Assay of the TR−DNA Interaction. The anisotropy binding titration assay of TR−DNA binding was performed by titration of varying amounts of TR (concentration range from 1 to 1000 nM, expressed as TR monomers) into a 10 nM solution of DNA−FITC. For all measurements, the maximal dilution was $<20\%$ and the fluorescence intensity was corrected for dilution of either DNA or TR concentration. All anisotropy binding titrations were conducted at 10 °C in 50 mM NaCl, 20 mM Hepes (pH 8.0), 3 mM dithiothreitol, and 5% glycerol. Additionally, to assess nonspecific binding, these assays were performed both in the absence and in the presence of 1 mM $MgCl_2$.

Quantitative Thermodynamic Analysis of Binding Equilibria. TR−DNA interaction isotherms were analyzed by two methods, as follows.

(*i*) *Model-Independent Binding*. The TR−DNA interactions were analyzed assuming a simple two-state reversible equilibrium between TR monomers and DNA. The dissociation constant (K_d) of this reaction can be described according to

$$K_d = (D \times \mathrm{TR})/\mathrm{TRD} \quad (3)$$

where D is the molar concentration of the free double-stranded DNA binding site, TR is the molar concentration of the free TR dimer, and TRD is the molar concentration of the complex formed between dimeric TR and DNA. The complex is related to the anisotropy measurements by

$$\mathrm{TRD} = D_t\alpha \quad (4)$$

and

$$\alpha = (A_{obs} - A_i)/(A_f - A_i) \quad (5)$$

where D_t is a total DNA concentration, α is the fraction of bound DNA, A_{obs} is the observed anisotropy at total monomeric protein concentration TR, and A_i and A_f are the lower and upper asymptotic limits, respectively, for anisotropy values obtained by fitting the curves. Then, it follows that

$$A_{obs} = A_i + (A_f - A_i)\{[(\mathrm{TR} + n)/(k^n)]/[1 + (\mathrm{TR}^n/k^n)]\} \quad (6)$$

where n is the Hill cooperativity coefficient and k is the K_d value (*32*, *33*).

In this work, we aim to characterize the hierarchical preference for TR−TRE binding. In this context, the difference in the overall change in Gibbs free energy (ΔG) derived from the apparent K_d, taken from protein binding to a reference TRE, provides a relative measure of differences in affinity and, thus, differential energetics of recognition. The Gibbs free energy change for the TR−TRE dissociation event (ΔG^0_{diss}) can be calculated from

$$\Delta G^0_{diss\text{-}HILL} = -RT \ln K_{diss} \quad (7)$$

where R is the gas constant and T is the assay temperature in kelvin.

No corrections were applied to quantum yields since no significant changes in fluorescence intensity occurred. The data were fitted using nonlinear least-squares regression analysis contained within SigmaPlot 2006 (version 10.0, Jandel Scientific Co.).

(*ii*) *Global Analysis*. We also fit the data using BIOQES (*34*−*36*), which uses implemented numerical solver-based binding data global analysis. BIOEQS allows the analysis of models containing multiple subunit equilibria that may include different oligomeric species, in various states of binding. The free energies recovered from BIOEQS correspond to dissociation free energies of each postulated species (e.g., monomer−DNA complex) from free elements (free monomer and free DNA) (*37*).

The model used to fit the multiple TRE binding profiles (intermediary model) was a system in which a protein binds to DNA in both a 1:1 and a 2:1 monomer−DNA complex ([TR−TRE] and [TR_2−TRE). Thus, the first free energy in the model, ΔG_1, is the dissociation free energy for the 1:1 monomer−DNA complex (here termed TR−TRE) for the free monomer (TR) and free DNA (TRE). The value of the second free energy, ΔG_2, corresponds to the dissociation free energy of the 2:1 monomer−DNA complex (here termed TR_2−TRE), also resulting in free monomer (TR) and free DNA (TRE). The dissociation free energy of the second monomer is $\Delta G_{2-1} = \Delta G_2 - \Delta G_1$. The observable values of the free TRE and of TR_2−HRE were set to the initial and final plateau values for the anisotropies, and these were considered as floating parameters.

Two types of fitting were conducted for the binding experiments: a one-species two-state fitting (TR−TRE or TR_2−TRE) and the two-species fitting mentioned above. Uncertainties of the recovered parameters were estimated at the 67% confidence limit (one standard deviation) using rigorous confidence limit testing in which, for each value for each parameter tested, the data were reanalyzed, allowing all of the other parameters to vary (covariance analysis) (*34*−*37*). To compare the Hill and global analysis (BIOEQS) approaches, we calculated the apparent dissociation free energy ΔG^0_{diss} from the K_d calculated by the independent model analysis (eq 7; $\Delta G^0_{diss\text{-}HILL}$) and the ΔG_{app} from BIOEQS ($\Delta G^0_{diss\text{-}GLOBAL} = {}^1/_2\Delta G_2$, as described in ref *37*).

For some curves with a highly apparent cooperative profile (with the total binding event occurring between 1 and 1.5 log units approximately, and/or when the two-species fitting has recovered a significant difference between ${}^1/_2\Delta G_2$ and ΔG_{2-1}), a third extremely cooperative fitting was conducted in BIOEQS.

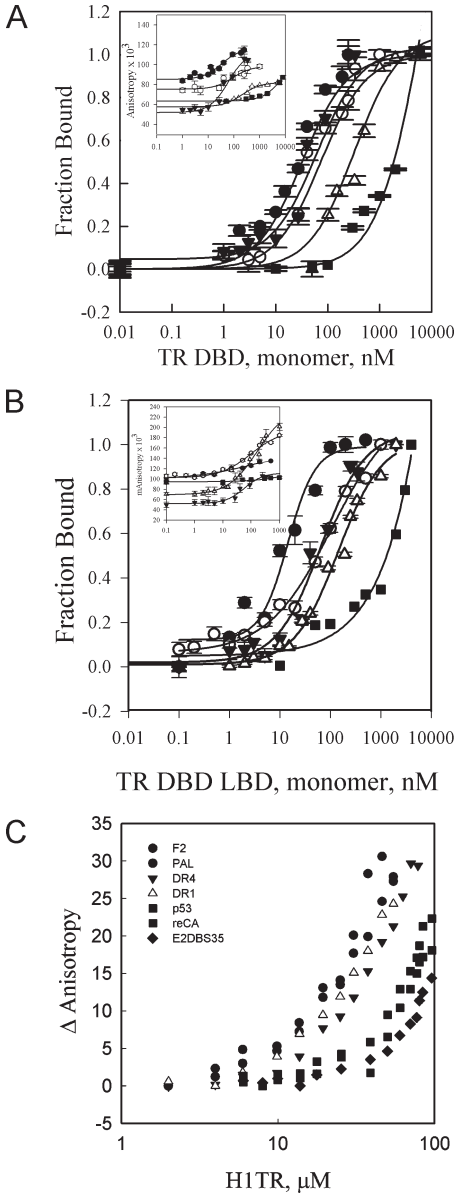

FIGURE 1: Fluorescence anisotropy curves for binding of TR DBD, TR DBD-LBD, and H1TR to DNA in the absence of $MgCl_2$. (A) Binding of TR DBD to F2 (●), PAL (○), DR-4 (▼), DR-1 (△), and a nonspecific DNA sequence p53 (■). (B) Binding of TR DBD-LBD to F2 (●), PAL (○), DR-4 (▼), DR-1 (△), and a nonspecific DNA sequence p53 (■). (C) Binding of peptide H1TR to specific TREs [F2 (◆), PAL (gray circles), DR-4 (gray triangles), and DR-1 (△)] and to nonspecific DNA sequences [p53 (dark gray squares), reCA (gray squares), and E2DBS35 (◆)].

In this fitting, we adopted an "all or nothing" model in that a monomer in solution binds DNA exclusively like a dimer (TR_2−TRE), without the presence of the monomeric intermediate (TR−TRE). The quality of the fitting was judged by the total χ^2 for each model (Supporting Information).

Structural Models. The only currently available crystallographic structure of TR DBD bound to DNA is that of the heterodimer of TR−RXR DBDs bound to DR4 [Protein Data Bank (PDB) entry 2NLL (*38*)]. Therefore, we built TR−TRE structural models to illustrate the possible organization of TR DBDs bound to the four different DNA arrays analyzed in this study. As a first step, the four DNA double-stranded TREs (F2, PAL, DR-4, and DR-1) were modeled using 3DNA (*39*). The TR DBD in PAL arrangement was prepared by superposing the

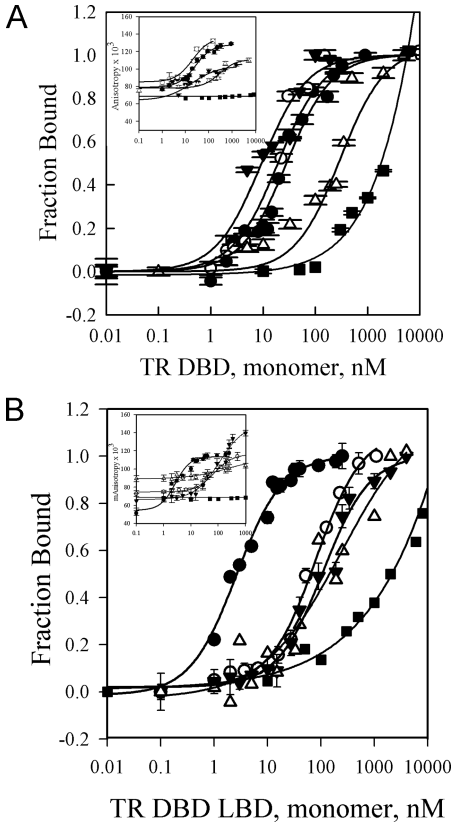

FIGURE 2: Fluorescence anisotropy curves for binding of TR DBD and TR DBD-LBD to DNA in the presence of 1 mM $MgCl_2$. (A) Binding of TR DBD to F2 (●), PAL (○), DR-4 (▼), DR-1 (△), and a nonspecific DNA sequence p53 (■) in the presence of $MgCl_2$. (B) Binding of TR DBD-LBD to F2 (●), PAL (○), DR-4 (▼), DR-1 (△), and a nonspecific DNA sequence p53 (■) in the presence of $MgCl_2$.

separated TR DBD on the crystal structure of ER DBDs complexed with a palindromic sequence [PDB entry 1HCQ (*40*)], respecting the interfaces observed in the ER structure. The TR−F2 model was built using the same template [PDB entry 1HCQ (*40*)], which was rotated, translated, and superimposed in the new DNA array (F2). The TR−RXR crystal structure [PDB entry 2NLL (*38*)] was used as a template for the TR−DR-4 model, in which the second TR DBD was superimposed onto the RXR DBD. Finally, the TR−DR-1 model was produced by the superposition of TR DBDs onto the RXR−RAR DBD crystal structure [PDB entry 1DSZ (*41*)]. All superpositions were accomplished using CCP4 (*42*). After being modeled, the PDB files were examined using Coot (*43*), to detect clashes and possible steric impediments. In the TR−DR-1 model, helix 1 had to be turned almost 180°, to prevent steric clashes in the structure.

RESULTS

To characterize the TR domains that affect the recognition and specificity of interaction with TRE DNA, we performed an anisotropy binding titration assay using the four canonical DNA responsive elements associated with TR binding. We used fluorescence anisotropy of fluorescein-labeled oligonucleotides, which provides a direct measure of the overall DNA hydrodynamic radius. The use of fluorescence anisotropy methods in measurements of binding events has some advantages as compared to other physicochemical methods. This method allows direct measurement of events at equilibrium in a well-controlled solution, without the co-additive and matrix effects common to

Table 1: Quantitative Analysis of the Interaction of TR DBD and TR DBD-LBD with TRE (F2, PAL, DR-4, and DR-1) Complexes in the Absence of Mg^{2+} Ions

	TR DBD			TR DBD-LBD		
TRE	K_d (nM)	Hill n	$\Delta G^0_{diss\text{-}HILL}$[a] (kcal mol^{-1} K^{-1})	K_d (nM)	Hill n	$\Delta G^0_{diss\text{-}HILL}$[a] (kcal mol^{-1} K^{-1})
F2	30.6 ± 5.7	1.2 ± 0.2	9.72 ± (1 × 10^{-5})	12.5 ± 7.5	1.6 ± 0.4	10.22 ± (6 × 10^{-6})
PAL	58.6 ± 12.8	1.2 ± 0.3	9.35 ± (4 × 10^{-5})	56.5 ± 13	1.3 ± 0.3	9.37 ± (3 × 10^{-5})
DR-4	76.5 ± 16.8	1.3 ± 0.1	9.20 ± (5 × 10^{-5})	63.1 ± 12	1.4 ± 0.2	9.31 ± (4 × 10^{-5})
DR-1	321.5 ± 72.9	1.0 ± 0.2	8.40 ± (4 × 10^{-4})	161.2 ± 29	0.9 ± 0.1	8.79 ± 0.0039

[a] $\Delta G^0_{diss\text{-}HILL}$ calculated from eq 7.

Table 2: Quantitative Analysis of the Interaction of TR DBD and TR DBD-LBD with TRE (F2, PAL, DR-4, and DR-1) Complexes in the Presence of 1 mM $MgCl_2$

	TR DBD			TR DBD-LBD		
TRE	K_d (nM)	Hill n	ΔG_{diss}[a] (kcal mol^{-1} K^{-1})	K_d (nM)	Hill n	ΔG_{diss}[a] (kcal mol^{-1} K^{-1})
F2	24.7 ± 3	1.6 ± 0.2	9.80 ± (8 × 10^{-6})	2.6 ± 1.6 (15 ± 2.0)[b]	1.6 ± 0.3	11.12 ± (9 × 10^{-7})
PAL	17.4 ± 3.7	1.5 ± 0.4	10.04 ± (6 × 10^{-6})	70 ± 6.8	1.3 ± 0.1	9.27 ± (4 × 10^{-5})
DR-4	9.8 ± 3.5	1.1 ± 0.04	10.36 ± (3 × 10^{-6})	88.3 ± 15.1	1.4 ± 0.2	9.01 ± (9 × 10^{-5})
DR-1	298.3 ± 56.4	1.0 ± 0.4	8.44 ± (3 × 10^{-4})	106.3 ± 33.5	0.9 ± 0.1	8.59 ± (2 × 10^{-4})

[a] $\Delta G^0_{diss\text{-}HILL}$ calculated from eq 7. [b] Calculated by interpolation of linear regression as shown in the inset of Figure 4.

the gel retardation assay or plasmon surface resonance (*30*). All TR constructs bind the tested fluorescein-labeled DNAs, as judged by the progressive increase in fluorescence anisotropy values as a function of peptide or protein concentration (Figures 1 and 2).

First, we proceeded with screening of two different TR constructs (TR DBD and TR DBD-LBD). Data from all performed anisotropy binding titration assays were analyzed employing both a noncooperative tight-binding model and a model-free Hill-based cooperativity analysis of interaction (details in Experimental Procedures). Analyses of our data with either paradigm gave similar results in terms of dissociation constants. However, the Hill-based cooperativity analysis resulted in an apparent Hill coefficient (n) statistically different from unity for F2, PAL, and DR4 TREs and close to unity for DR1 (Tables 1 and 2 and Figures 1 and 2). These results indicate that TR binding to TREs displays cooperative behavior in binding some TREs (F2, PAL, and DR4) and noncooperative behavior for DR1 binding. This cooperative behavior revealed for TR-F2, DR4, and PAL binding is a clear indication that TR binds in these elements preferentially as dimers, since the first monomer binding improves the binding of the second one.

The K_d values determined here for TR DBD demonstrate that this domain is able to bind with similar high affinities to three of four studied TREs (30.6 nM for F2, 58.6 nM for PAL, and 76.5 nM for DR-4), whereas binding to DR-1 occurred with a lower affinity (321.5 nM) (Table 1 and Figure 1A).

The presence of LBD practically did not change the K_d values for PAL and DR-4 [56.5 and 63.1 nM, respectively (Table 1 and Figure 1B). However, the TR DBD-LBD−DR-1 affinity was somewhat improved (161.2 nM), although this element still has the lowest binding affinity for TRE. Furthermore, the affinity of LBD-DBD for the F2 element, determined in an independent study, also was better (12.5 nM) as compared to that for binding of TR LBD to the same TRE. Interestingly, the cooperativity of the binding does not change in the presence of LBD; however, it changes with the DNA array in analysis. These results indicate that the DBD domain is capable of binding to different TREs, whereas the addition of LBD interferes with the process of DNA recognition. Such interference affects binding of TR to TREs organized as direct repeats or palindromes. In other words, the DBDs recognize and bind to AGGTCA half-site motifs, and addition of LBD causes the binding to become more specific. Its presence imposes structural restrictions on the interactions of the LBD homodimer interface with DBD arrangements on DNA, improving the affinity between TR and TREs F2 and DR1.

The free energies calculated with BIOEQS were very similar to those calculated from Hill fitting, considering the absolute values and the errors (Table 3 and Figure 3), and validating the data in both analyses. It was possible to evaluate the same tendency in TR DBD-LBD or TR DBD preferences for the TREs. For each TR construct and each TRE in the presence or absence of Mg^{2+}, we fitted the data following two models: a two-state model and an intermediary model (described in Experimental Procedures). All the data fit well to the models, except for the TR DBD-LBD−F2 combination in the presence of Mg. The binding of TR DBD-LBD to F2 manifests itself as a high-affinity curve, and it was fitted only as a two-state model, which could mean monomers or dimers binding to F2. According to our data (Table 3), it was not possible to differentiate between two-state and intermediary models for TR DBD-LBD with PAL, DR4, or DR-1; for F2 in the presence of Mg, the best fitting was provided by the intermediary model. For binding of TR DBD to F2 and DR-1, in the absence of Mg, and to PAL, DR-4, and DR-1, in the presence of Mg, the best fittings were cooperative. Although the χ^2 value comparison slightly favored the cooperative or intermediary model of TR DBD− and DBD-LBD−TRE binding [except for DR-1 (data not shown)], the quality of the data does not provide a possibility to choose one of these two models (two-state or intermediary model).

All the measured data, except for those for TR DBD with DR1 in the absence of Mg^{2+}, presented satisfactory χ^2 values (Table 1 of the Supporting Information). The comparison between the χ^2 values for each model shows some preference for cooperative

Table 3: Recovered $\Delta G^0_{\text{diss-GLOBAL}}$ Values[a] and Parameters Calculated via BIOEQS Analyses for TR DBD-LBD and TR DBD with and without $MgCl_2$

	without Mg^{2+}							with 1 mM Mg^{2+}						
	ΔG_1[b]	ΔG_2[b]	χ^2[c]	ΔG^{2d}	χ^2[c]	ΔG_c[e]	χ^2[c]	ΔG_1[b]	ΔG_2[b]	χ^2[c]	ΔG^{2d}	χ^2[c]	ΔG_c[e]	χ^2[c]
TR DBD-LBD−F2	11.44 (1.0, −0.7)	20.20 (1.0, −0.8)	1.47	9.73 (0.5, −0.6)	2.85	ND[f]	ND[f]	ND[f]	ND[f]	ND[f]	11.77 (0.6, −0.4)	4.57	ND[f]	ND[f]
TR DBD-LBD−PAL	9.85 (0.3, −0.4)	18.41 (0.3, −0.4)	2.96	9.24 (±0.2)	2.83	ND[f]	ND[f]	9.57 (0.2, −0.30)	18.73 (0.17, −0.15)	0.21	9.28 (±0.1)	0.29	ND[f]	ND[f]
TR DBD-LBD−DR-4	9.72 (0.4, −1.0)	18.96 (0.4, −0.3)	0.30	9.37 (0.2, −0.2)	0.28	ND[f]	ND[f]	9.56 (0.4, −0.4)	18.03 (0.3, −0.3)	0.98	8.99 (0.2, −0.2)	0.94	ND[f]	ND[f]
TR DBD-LBD−DR-1	9.49 (0.1, −0.2)	17.77 (0.2, − 0.2)	0.58	8.84 (0.1, −0.1)	0.69	ND[f]	ND[f]	9.69 (0.6, −0.9)	17.38 (< 18.6)	0.3	8.98 (0.5, −0.5)	0.30	ND[f]	ND[f]
TR DBD−F2	0.46 (< 0.7, −2.5)	20.31 (1.2, −0.8)	5.46	9.8 (0.6, −0.6)	5.73	20.32 (1.2, −0.6)	4.8	10.51 (0.4, −0.3)	20.1 (0.4, −0.3)	2.17	9.91 (0.2, −0.2)	2.01	ND[f]	ND[f]
TR DBD−PAL	9.47 (0.7, −2.5)	18.25 (0.6, −0.72)	0.88	8.99 (±0.4)	0.77	18.44 (0.9, −0.7)	1.1	10.47 (< 11.8)	21.44 (0.2, −1.0)	2.80	10.20 (±0.4, −0.3)	2.77	20.92 (0.6, −0.5)	2.4
TR DBD−DR-4	9.86 (< 10.6)	19.23 (0.4, −0.8)	1.83	9.45 (0.2, −0.2)	1.67	19.3 (0.4, −0.3)	2.1	1.22 (< 11.12)	19.61 (0.6, −0.9)	1.62	9.73 (0.5, −0.7)	1.29	19.63 (0.6, −0.8)	1.3
TR DBD−DR-1	8.09 (< 9.1)	17.07 (0.3, − 0.3)	167	8.48 (0.2, −0.2)	195.5	17.06 (0.2, −0.3)	143	8.24 (< 9.9)	16.91 (0.3, −0.3)	2.96	8.35 (0.3, −0.3)	2.91	16.92 (0.3, −0.2)	2.73

[a] Dissociation Gibbs free energy $\Delta G^0_{\text{diss-GLOBAL}}$ values in kilocalories per mole per kelvin. The uncertainties in the ΔG values were estimated by rigorous confidence tests of the parameters recovered in the fitting, according to ref 36. [b] ΔG_1 and ΔG_2 are dissociation free energies for the first (MD) and second (MMD) protein−DNA complex species, respectively (intermediary model). [c] χ^2 is the total χ^2 value recovered in the fitting. [d] ΔG^2 is the dissociation free energy recovered in the simple association (two-state model) fitting. [e] ΔG_c is the dissociation free energy recovered in the highly cooperative model. [f] Not determined.

and intermediary models in detriment to the two-state model, except for some TREs for which all the applied models led to similar results.

To evaluate the binding specificity of TR DBD and TR DBD-LBD with TREs, we also assessed binding of TR to a nonspecific DNA with a scrambled sequence, which had no similarity to the consensus AGGTCA motifs. Our results show that association of TR DBD-LBD and TR DBD with this sequence occurred only at very high protein concentrations (> 1.5 μM). This substantiates the notion that the interactions among TR and the TREs are specific (Figure 1A,B).

To investigate a minimum structural TR DBD element required for TRE recognition, we determined whether a short peptide corresponding to the DNA recognition helix of TR, H1TR, would be able to recognize and bind selectively to TRE. The DNA binding isotherms shown in Figure 1C indicate that all TREs were recognized by H1TR. DNA binding occurred in the micromolar range and achieved saturation with a peptide concentration of 100 μM, which is indicative of only a weak binding affinity. As expected, the minimum recognition peptide H1TR was not able to differentiate between different arrangements of the half-sites but was able to distinguish between DNA sequences composed of TR half-sites (AGGTCA) and other nucleotides, which do not contain this recognition sequence.

The ability of H1TR to discriminate between specific and nonspecific DNA was characterized using anisotropy binding titration assays. This was done with three different TR nonspecific DNAs, which are cognate sequence responsive for their original protein targets: p53 tumor suppressor [p53DBS (*44*)], LexA repressor from the *E. coli* SOS system [recA DNA (*45*)], and E2 repressor protein from papillomavirus [E2DBS (*32*)]. H1TR binding to these three DNA targets was weaker than to the TREs (Figure 1C). This implies that although the H1TR peptide cannot distinguish between different TREs, there is sufficient encoded structural information to discriminate between TR-specific and nonspecific DNA sequences.

Mg^{2+} Influences TR−DNA Specificity. Divalent cations at moderately low concentrations, in particular magnesium, play an important role in nucleic acid binding events, modulating both affinity and specificity in many different systems through specific interactions with DNA (*46*−*51*). In fact, Mg^{2+} has an extensive effect on DNA recognition by proteins through strong coordination of DNA and weakening nonspecific interactions. To evaluate a possible role for Mg^{2+} in the interaction of TR DBD and TR DBD-LBD with TREs, we performed the same DNA binding experiments as described above in the presence of $MgCl_2$ (Table 2and Figure 2).

For the TR DBD construct, Mg^{2+} practically did not influence its binding to F2 and DR-1. In the case of PAL and its binding to DR-4 response elements, we observed declines in the K_d values of approximately 3 and 8 times, respectively, induced by Mg^{2+}. This indicates that interactions of TR DBD with PAL and DR-4 are somewhat nonspecific and somewhat suboptimized in the absence of Mg^{2+}. On the other hand, with either Mg^{2+} or other divalent ions, such interactions could be improved. Indeed, interactions of TR DBD with TREs are preferentially enhanced by Mg^{2+}. The affinities (K_d) for F2, PAL, and DR-4 are 24.7, 17.4, and 9.8 nM, respectively. The DR-1 response element continues to display the lowest binding affinity for TR DBD (Table 2). These results suggest that the binding of TR DBDs to TREs is mostly guided by recognition of the AGGTCA half-sites, as reflected by their very similar K_d values, and these results agree

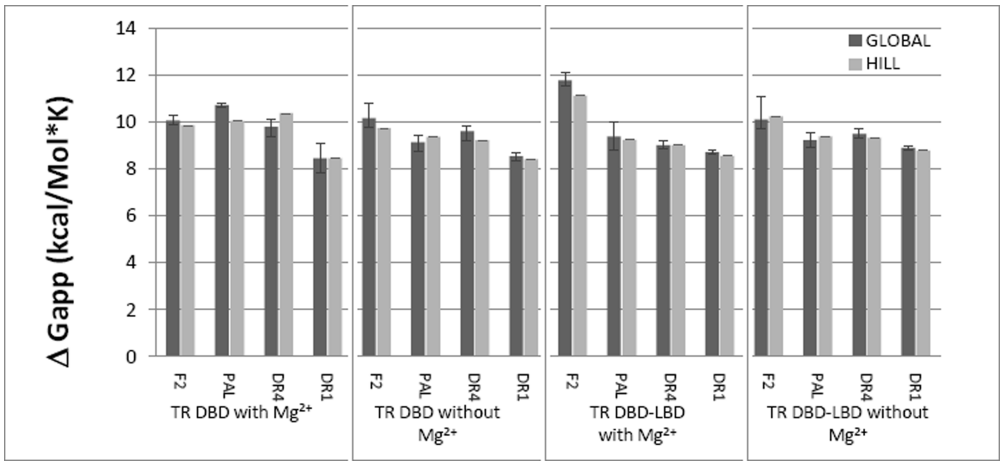

FIGURE 3: Comparison between ΔG^0_{diss} calculated from global analysis with BIOEQS (GLOBAL) and from Hill fitting (HILL) for TR DBD-LBD and TR DBD with and without 1 mM $MgCl_2$.

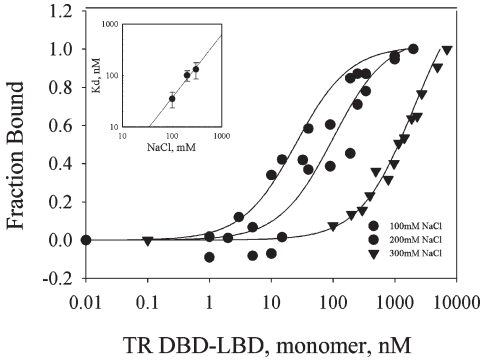

FIGURE 4: TR DBD-LBD−F2 binding interaction dependence on the ionic strength. Fluorescence anisotropy curves of binding the TR DBD-LBD to F2, in the presence of Mg^{2+}. The binding assays were performed at the following salt concentrations: NaCl at 100 mM (gray circles), 200 mM (gray triangles), and 300 mM (gray squares). The inset shows a plot of K_d vs NaCl concentration. The solid line is a first-order linear regression, used in the interpolation of the TR DBD-LBD−F2 K_d at 50 mM NaCl.

with global analysis of binding data determined with BIOEQS (Figure 3). Additionally, our results point out that the binding of TR DBD with DR-1 most probably has additional structural impediments (presumably because of the smaller separation between the two half-sites), which is reflected by its high K_d value and by its noncooperative behavior, which indicates that the monomers bind DNA independently.

We also performed TRE binding studies using the TR construct, which includes the ligand binding domain, TR DBD-LBD, in the presence of Mg^{2+}. Taking into consideration the error values, we found addition of Mg^{2+} did not significantly change the binding of TR DBD-LBD to any of the studied TREs, with F2 apparently being an exception (see below). This lack of interference caused by divalent Mg^{2+} in the binding of TR DBD-LBD to TREs is indicative of a higher specificity of TRE recognition for TR DBD-LBD (Tables 1 and 2). Taken together, these results confirm the preference of TR for binding to F2. Moreover, other tested TREs (PAL, DR-4, and DR-1) have a high, nanomolar range, affinity for TR DBD-LBD.

Characterization of TR DBD-LBD−F2 Binding Specificity. The apparent initial K_d for interaction of F2 with TR DBD-LDB at 50 mM NaCl in the presence of Mg^{2+} was found to be on the same order of magnitude as that of the DNA concentration used in our assays ($K_d = 2.6 \pm 1.6$ nM; [DNA] = 10 nM). Because of the proximity of these values, even the use of the tight binding model approach in the F2 binding curve analysis may not be adequate for avoiding significant errors. Therefore, we chose the Wyman binding linkage approach (*44*, *50*) as an alternative for the estimate of the TR DBD-LBD−F2 dissociation constant at low ionic strengths in the presence of Mg^{2+}.

Table 4: Dissociation Constants of the TR DBD-LBD−F2 Complex in the Presence of Varying NaCl Concentrations

[NaCl] (mM)	K_d (nM)
50	2 ± 1.6
100	35.3 ± 11.9
200	99.9 ± 23.5
300	131.0 ± 45.4

Monovalent cations (M^+) have considerable effects on the protein−DNA binding process by counterion shielding of DNA. Their presence results in a decrease in protein−DNA affinity with the increase in M^+ concentration, so that the log $K_{d,obs}$ function is linearly proportional to log[M^+] (*47*). An increase in the NaCl concentration progressively increased the TR DBD-LBD−F2 K_d value to 35, 100, and 130 nM at NaCl concentrations of 100, 200, and 300 mM, respectively (Figure 4 and Table 4). Assuming a linear dependence of log K_d on log[NaCl] (*48*), the K_d for the interaction of TR DBD-LBD with F2 at 50 mM NaCl is 15.4 nM (Table 2). According to this analysis, the K_d for formation of the TR DBD-LBD−F2 complex in the presence of Mg^{2+} is close to the K_d of the TR DBD-LBD−F2 complex in the absence of Mg^{2+} [12.5 ± 7.5 nM (Table 1)]. These results strengthen the idea that binding of TR DBD-LBD to F2 is highly specific and is independent of the presence of Mg^{2+}.

TR−DNA Binding Stoichiometry. We used the results of nondenaturing PAGE to determine the stoichiometry of binding of TR to TREs. Figure 5 shows that TR binds to different TREs as dimers. The differences among the band intensities in the gel are probably caused by variations in the TR affinity for each type of TRE: F2, PAL, DR-4, and DR-1. As revealed previously (*27*), the TR forms tetramers at high concentrations (>40 μM) in solution in the absence of its cognate ligand, T3. Addition of T3 leads to dissociation of TR tetramers into dimers available for TR activation. We confirmed that in absence of T3, the TR DBD-LBDs move as a slower band with an estimated

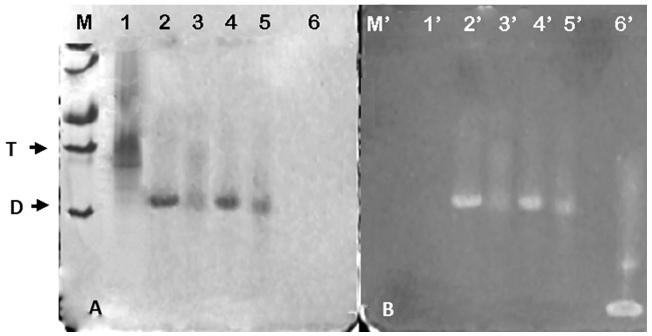

FIGURE 5: Gel retardation assay for binding of TR to DNA. Nondenaturant acrylamide gel electrophoresis of TR DBD-LBD (48 μM monomers) was performed in the absence and presence of four different TREs (24 μM each): F2, DR-4, PAL, and DR-1. The gel was stained with (A) Coomassie Brilliant Blue G-25 for determination of protein band position and (B) ethidium bromide to evidence the DNA migration: lanes 1 and 1′, TR DBD-LBD without DNA, as tetramers; lanes 2 and 2′, TR DBD-LBD with F2; lanes 3 and 3′, TR DBD-LBD with DR-4; lanes 4 and 4′, TR DBD-LBD with PAL; lanes 5 and 5′, TR DBD-LBD with DR-1; and lanes 6 and 6′, free TRE F2, as a control. We can notice that the binding of the three last DNAs, the binding of TR-TREs is better than the last one, which can be seen by the more defined bands that correspond to protein (3 to 5) and to DNA (3′ to 5′). The blurred bands decrease in intensity from lane 2′ to 5′, with species that correspond to tetramers (calculated R_h = 4.1 nm) and dimers (calculated R_h = 3.6 nm). The R_h values were calculated with the retardation factor (R_f) of each protein used as standard, which were plotted as $100[\log(100R_f)]$ vs R_h. The first-order regression function obtained from this plot (not shown) was used to calculate the R_h of TR dimer-bound DNA (D) and TR tetramers (T). (C) Stoichometry curves for binding of TR DBD-LBD and TR DBD to F2. To better elucidate the results, the protein concentration was divided by the TRE concentration used in the assay. The observed stoichiometry is two TRs for each HRE molecule.

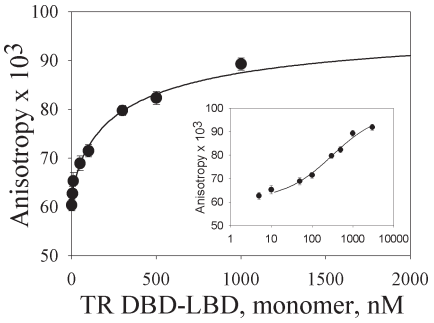

FIGURE 6: Anisotropy binding titration assay for TR dimerization studies. Determination of dissociation constants for TR dimers was performed by a fluorescence anisotropy assay of fluorescein-labeled TR (TR−FITC), as described in Experimental Procedures. Plot of TR DBD-LBD association in linear scale and in logarithmic scale (inset).

hydrodynamic radius (R_h) of 4.1 nm, which corresponds to TR tetramers (Figure 5A,B). When TR is bound to any of the four TREs, its migration in the nondenaturing PAGE was accelerated and the R_h was compatible to that of TR dimers (R_h = 3.6 nm). This migration pattern reveals that the tetramers dissociated into dimers in the presence of DNA, indicating a DNA binding event coupled to TR subunit rearrangements, as follows:

$$(TR)_4 + 2DNA \Leftrightarrow 2[(TR)_2 - DNA]$$

These data were further confirmed by determining the stoichiometric relationship between TR and TRE binding. This was done by performing fluorescence anisotropy measurements of fluorescein-labeled DNA in large excess of its unlabeled counterpart. Our data reveal that both TR DBD-LBD and TR DBD bind to F2, DR-4, PAL, and DR-1 as dimers (Figure 5C). Also, the model fitted using BIOEQS has shown that most of the best fitting follows the intermediary or cooperative model, indicating more than one species in solution.

On the other hand, in the low nanomolar range, TR DBD-LBDs already present a marked change in the monomer−dimer balance (Figure 6), with a K_d of 154.7 ± 45 nM. As a consequence, at concentrations of >150 nM, the TR DBD-LBD construct will predominantly form dimers. Since the binding affinities of TR-DBD-LBD for TREs are all in the range of the K_d value of TR dimerization, it is plausible to assume that TR DBD-LBDs recognize and bind DNA simultaneously with dimerized TR. Additional evidence for binding of TR to DNA as dimers is provided by the Hill coefficient n (eq 6) (Tables 1 and 2), indicating positive cooperativity, in a different degree for each particular TRE. Thus, we propose that bimolecular events take place in solution and that any small amount of free monomeric TR species binds to DNA, with high affinity, in cooperative fashion. Tetrameric dissociation coupled to DNA binding is unlikely to occur under physiological conditions, since nuclear receptors are usually found in cells in the nanomolar range. Collectively, these data provide a clear indication of a direct DNA binding event by free TR dimers, or by cooperative binding of TR monomers to DNA coupled to protein dimerization. These results corroborate a previous report that revealed that the TRβ full-length receptor binds to DR-4 and palindromic sequences (such as PAL and F2) as homodimers and that T3 binding induces TR dissociation followed by heterodimerization with RXR (*20*, *26*, *27*, *51*).

DISCUSSION

TR is involved in several important physiological processes, which are mediated by DNA recognition and modulated by ligand binding (*1*, *2*, *11*, *14*). Although TR response elements have been extensively studied in vitro, little is known about the types of interactions that can occur between different TR constructs and TREs. This study has shed light on this question by using analytical biophysical techniques to characterize the binding constants of the interactions among these complexes.

The actual activity of protein samples, i.e., the fraction of folded, active protein, which is sometimes difficult to ascertain, was confirmed here by three different techniques: (i) gel shift mobility assay (Figure 5) with DNA responsive elements (notice the complete migration of the free DNA to a bound DNA form upon complexation), (ii) anisotropy assay of DNA binding under stoichiometric conditions (Figure 6), and (iii) independent small-angle X-ray scattering studies (results not shown). Our results clearly show that TRs bind to TREs with a 2:1 stoichiometry. Furthermore, the fluorescence anisotropy results suggest that TR DBD interaction conveys structural information causing TREs to bind with similar affinities to F2, PAL, and DR-4. Addition of Mg^{2+} reduced the level of nonspecific DNA binding, leading to smaller differences in the interaction of TR DBD with TREs (Tables 1 and 2). Indicative of the Mg^{2+} effect is the fact that the K_d values for the interaction of F2, PAL, and DR-4 with TRE were very similar to one another; DR-1 is the only response element that had a lower binding affinity for TR DBD, noncooperative binding, and a significantly different K_d, probably because of the short separation between the two half-sites, which

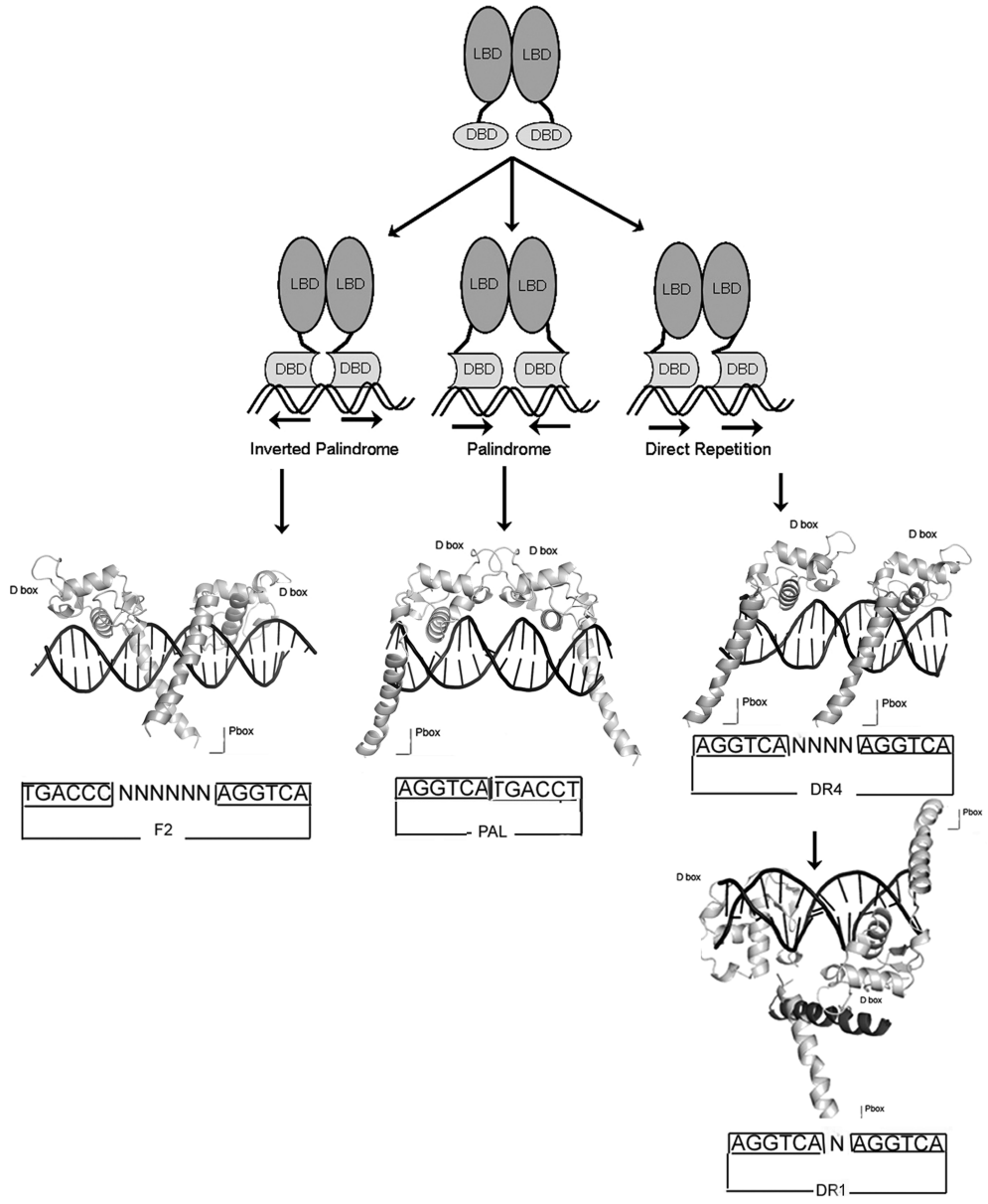

FIGURE 7: Schematic model for TR regulation through different responsive elements. The TR homodimers can bind to different arrays of TREs: inverted palindromes (F2), palindromes (PAL), and direct repetitions (DR-4 and DR-1). Models of the positions of DBDs in the DNA interaction. In F2m the DBDs show a different dimerization interface with the hinges crossing. The binding to PAL reveals the cited dimerization interface to ER (*45*). The DR-4 interaction shows the same array of the TR−RXR heterodimer (*47*). In DR-1, helix a (dark gray) must be repositioned (light gray) to better interact with the DNA and to avoid clashes in the structure.

prevented the correct binding of two independent TR DBD monomers.

LBD imposed some structural restrictions on binding of TREs to PAL, DR-4, and DR-1. This change suggests that LBD enhanced the specificity of F2 recognition, presumably by positioning the DBDs in the appropriate orientation and separation from one another (Tables 1 and 2). Moreover, the dimerization interface imposed by LBD stabilized the repertoire of possible binding sites dictated by DBD (*26*, *52*, *53*). Additionally, the preferential hinge positioning may have imposed a TR specific conformation, which also contributed to a better binding of TR to F2 than to other TREs. Accordingly, our preliminary data indicate that the TRα protein fragment, which contained the DBD and part of the D domain−hinge motif, also dimerized in solution. Thus, protein−protein interactions at the LBD also seemed to influence the position and/or conformation of the D domain (*54*). Such reorganization corroborates our previous findings of D domain rearrangements in high-resolution X-ray crystallographic structures of TRβ and TRα isoforms and suggests that these interactions could provide rotational flexibility required for recognition of specific DNA elements such as F2 (*54*). Also, our TR DBD-LBD low-resolution models notably showed that the TR DBDs were closely juxtaposed to one another, allowing the D domain−hinge regions to interact with one another. This close juxtaposition of DBDs and hinge domains in the TRs raises the possibility that these regions engage in homodimer specific contacts that strengthen LBD−LBD interactions and help to position the DBDs in an F2 configuration for DNA binding (*28*).

Our results also support the notion that minimal domains of TR such as the H1TR fragment, with a low degree of structural information and complexity, also can recognize the TREs, but in a nonspecific way. TRE discriminatory capacity is enhanced when it binds to full-length DBD and heightened further when

LBD was present. Studies performed with the full-length ER and ER DBD showed binding profiles between each of these two protein constructs and DNA that are very similar to our results for the TR interaction. This agreement indicates that selectivity increased when the protein was its full size (*55*). Furthermore, the three-dimensional structure of the full-length receptor complex formed by PPAR, RXR, and DR1 revealed additional contacts between the LBD of PPAR and the DBD of RXR, which might explain the importance of having LBD present for DNA recognition (*56*).

TR−DNA Binding and Structural Information. To improve our understanding of the structural basis of TR−DNA recognition, we analyzed putative three-dimensional models of TR DBDs bound to TREs. These models are based on the crystallographic structures of the DBD−DNA complexes with different TREs. Figure 7 shows that for the palindromic array (PAL), the dimerization interface is formed by the D-boxes, containing the first zinc finger, while the P-box establishes the selective base of the contacts in the major groove of DNA. Hence, the structure is more compact mainly due to the lack of the spacing between the motifs. Our structural model of TR superposed on the ER DBD crystal structure and complexed with a palindromic sequence [PDB entry 1HCQ (*40*)] (Figure 7) indicates that the short length of PAL does not require significant DNA structural deformations for the formation of the TR DBD−TRE complex. The K_d affinity values obtained for the interaction of TR DBD with PAL support this notion. However, addition of the LDB domain decreased the affinity of TR DBD-LBD for PAL. Such a decline is most probably because of minimal or no interactions on the TR LBD homodimeric interface in this setting, as implicated by our binding studies.

The model of binding of TR to F2, generated by rotation and translation of the TR−PAL model, shows that the DBD classical dimerization interface is not preserved. However, the dimerization interface could be maintained in the LBD portion of the protein, because of the flexibility of its hinge regions and their ability to cross. Furthermore, since the spacing between the two AGGTCA half-sites is composed of 6 bp, it presumably accommodates the DBDs better in a conformation, which favored DNA TRE recognition. This led to a smaller K_d value for binding of TR to F2. Moreover, the SAXS model of TR DBD-LBD reveals that crossing of the hinges (D-domains) provides the best mutual positioning of TR LBD and DBD domains within the low-resolution SAXS envelope (*28*). The TR DBDs in this case are in a position and orientation that is best suited for F2 recognition (*28*). This sheds light on the structural basis for preferential binding of TR DBD-LBD to TRE.

Direct repeats are less efficient DNA targets for TR homodimers (*28*, *49*, *55*). The crystal structure of TR-RXR DBDs bound to DR-4 [PDB entry 2NLL (*38*)] revealed that the first zinc finger region of TR (3′) interacts with the second RXR (5′) zinc finger to promote a selective binding to the direct repeat (*38*). In this structure, the DNA region where RXR binds suffers a deformation, which probably could be reverted by Mg^{2+} coordination through improved binding. The latter effect has been observed in our experiments. Here we presume that the same structural interactions are maintained in the TR DBD−DR-4 complex.

The TR-DBD−DR-1 model, produced by the superposition of TR DBDs onto the RXR−RAR DBD crystal structure [PDB entry 1DSZ (*41*)], reveals that DBD helix 1, containing the hinge region, must suffer a dramatic conformational rearrangement, by turning almost 180°, to allow TR to bind to DR-1 as dimers. In other words, it was structurally impossible to allow the required spacing for adequately positioning the α-helix and, at same time, to maintain the LBD dimerization interface. This is consistent with our determination of a poor affinity of TR for DR-1.

In conclusion, our results revealed that a more complete TR structure was better able to discriminate among preferential TREs. Although our data revealed that the TR DBD-LBD complex has a high preference for binding to TRE F2, we also found that apo-TR DBD-LBD bound with high affinity to the other canonical TREs, such as PAL, DR-4, and DR-1, albeit with lower affinity. We clearly show that the degree of TR structure completeness affects the amount of encoded information for DNA binding, which plays a key role in determining the extent of recognition and specificity of TREs binding to TR. TR structural intactness enhanced its binding to F2 and also modulates recognition of PAL, DR-4, and DR-1 elements. On a molecular level, the introduction of LBD imposed steric restrictions via the hinge (D-domain), preventing high-affinity binding to the latter TREs. The K_d values for three different TR constructs with four different TREs, which include various arrangements of G/AGGTC motifs (F2, PAL, DR-4, and DR-1), are consistent with the predictions of the proposed structural models. These K_d values are also in agreement with those obtained for NRs by other techniques (*26*, *51*, *57*−*59*).

ACKNOWLEDGMENT

We acknowledge the kind donation of human TR DBD-LBD clones from John Baxter's laboratory, at The Methodist Hospital (Houston, TX), the TR DBD expression and purification by Mario de Oliveira Neto, and Dr. Peter Reinach for his help with the preparation of the manuscript.

SUPPORTING INFORMATION AVAILABLE

Comparison of data between all experimental treatments in Supporting Information, including χ^2 values for each model (intermediate, two-state, and cooperative) used in global analysis (Table 1) and all ΔG values for dissociation free energies for intermediary, two-state, and cooperative models recovered by global fittings and calculated apparent ΔG values from global and Hill analyses (Table 2). This material is available free of charge via the Internet at http://pubs.acs.org.

REFERENCES

1. Aranda, A., and Pascual, A. (2001) Nuclear Hormone Receptors and Gene Expression. *Physiol. Rev. 81*, 1270–1295.
2. Yen, P. M., and Chin, W. W. (1994) Molecular Mechanisms of Dominant Negative Activity by Nuclear Hormone Receptors. *Mol. Endocrinol. 8*, 1450–1454.
3. Berglund, H., Wolf-Watz, M., Lundback, T., van den Berg, S., and Hard, T. (1997) Structure and dynamics of the glucocorticoid receptor DNA-binding domain: Comparison of wild type and a mutant with altered specificity. *Biochemistry 36*, 11188–11197.
4. Klug, A., and Schwabe, J. W. (1995) Protein motifs 5: Zinc fingers. *FASEB J. 9*, 597–604.
5. Nagaya, T., and Jameson, J. L. (1993) Distinct dimerization domains provide antagonist pathways for thyroid hormone receptor action. *J. Biol. Chem. 268*, 24278–24282.
6. Lazar, M. A., Berrodin, T. J., and Harding, H. P. (1991) Differential DNA binding by monomeric, homodimeric, and potentially heteromeric forms of the thyroid hormone receptor. *Mol. Cell. Biol. 11*, 5005–5015.
7. Mangelsdorf, D. J., Thummel, C., Beato, M., Herrlich, P., Schiitq, G., Umesono, K., Blumberg, B., Kastner, P., Mark, M., Chambon, P., and Evan, R. M. (1995) The nuclear receptor superfamily: Second decade. *Cell 83*, 835–839.

8. Samuels, H. H., Forman, B. M., Horowitz, Z. D., and Ye, Z.-S. (1988) Regulation of gene expression by thyroid hormone. *J. Clin. Invest. 81*, 957–967.
9. Brent, G. A., Harney, J. W., Chen, Y., Warne, R. L., Moore, D. D., and Larsen, P. R. (1989) Mutations of the rat growth hormone promoter which increase and decrease response to thyroid hormone define a consensus thyroid hormone response element. *Mol. Endocrinol. 3*, 1996–2004.
10. Tagami, T., Madison, L. D., Nagaya, T., and Jameson, J. L. (1997) Nuclear receptor corepressors activate rather than suppress basal transcription of genes that are negatively regulated by thyroid hormone. *Mol. Cell. Biol. 17*, 2642–2648.
11. Glass, C. K. (1996) Some new twists in the regulation of gene expression by thyroid hormone and retinoic acid receptors. *J. Endocrinol. 150*, 349–357.
12. Wu, Y., Xu, B., and Koenig, R. J. (2001) Thyroid hormone response element sequence and the recruitment of retinoid X receptors for thyroid hormone responsiveness. *J. Biol. Chem. 276*, 3929–3936.
13. Piedrafita, J. F., Ortiz, M. A., and Pfahl, M. (1995) Thyroid hormone receptor homodimers can function as ligand-sensitive repressors. *Mol. Endocrinol. 9*, 563–578.
14. Evans, R. M. (1988) The steroid and thyroid hormone receptor superfamily. *Science 240*, 889–895.
15. Umesono, K., Murakami, K. K., Thompson, C. C., and Evans, R. M. (1991) Direct repeats as selective response elements for the thyroid hormone, retinoic acid, and vitamin D3 receptors. *Cell 65*, 1255–1266.
16. Williams, G. R., and Ga, B. (1995). Thyroid hormone response elements. In Molecular endocrinology: Basic concepts and clinical correlations (Weintraub, B. D., Ed.) pp 217−239, Raven Press, New York.
17. Ribeiro, R. C. J., Apriletti, J. W., Wagner, R. L., West, B. L., Feng, W., and Huber, R. (1998) Mechanisms of thyroid hormone action: Insights from X-ray crystallographic and functional studies. *Recent Prog. Horm. Res. 53*, 351–394.
18. Rosenfeld, R. M. (1987) A c erb-A binding site in rat growth hormone mediates trans-activation by thyroid hormone. *Nature 329*, 738–741.
19. Glass, C. K., Holloway, J. M., Devary, O. V., and Rosenfeld, M. G. (1988) The thyroid hormone receptor binds with opposite transcriptional effects to a common sequence motif in thyroid hormone and estrogen response elements. *Cell 54*, 313–323.
20. Yen, P. M. (2001) Physiological and molecular basis of thyroid hormone action. *Physiol. Rev. 81*, 1097–1142.
21. Bugge, T. H., Pohl, J., Lonnoy, O., and Stunnenberg, H. G. (1992) RXRα, a promiscuous partner of retinoic acid and thyroid hormone receptors. *EMBO J. 11*, 1409–1418.
22. Kliewer, S. A., Umesono, K., Mangelsdorf, D. J., and Evans, R. M. (1992) Retinoid X receptor interacts with nuclear receptors in retinoic acid, thyroid hormone and vitamin D3 signalling. *Nature 355*, 446–449.
23. Leid, M., Kastner, P., Lyons, R., Nakshatri, H., Saunders, M., Zacharewski, T., Chen, J. Y., Staub, A., Gamier, J. M., Mader, S., and Chambon, P. (1992) Purification, cloning, and RXR identity of the HeLa cell factor with which RAR or TR heterodimerizes to bind target sequences efficiently. *Cell 68*, 377–395.
24. Zhang, X. K., Hoffmann, B., Tran, P. B. V., Graupner, G., and Pfahl, M. (1992) Retinoid X receptor is an auxiliary protein for thyroid hormone and retinoic acid receptors. *Nature 355*, 441–446.
25. Miyamoto, T., Suzuki, S., and DeGroot, L. J. (1993) High affinity and specificity of dimeric binding of thyroid hormone receptors to DNA and their ligand-dependent dissociation. *Mol. Endocrinol. 7*, 224–231.
26. Ribeiro, R. C., Kushner, P. J., Apriletti, J. W., West, B. L., and Baxter, J. D. (1992) Thyroid hormone alters in vitro DNA binding of monomers and dimers of thyroid hormone receptors. *Mol. Endocrinol. 6*, 1142–1152.
27. Figueira, A. C. M., Dias, S. M., Santos, M. A., Apriletti, J. W., Baxter, J. D., Webb, P., Neves, F. A., Simeoni, L. A., Ribeiro, R. C., and Polikarpov, I. (2006) Human thyroid receptor forms tetramers in solution, which dissociate into dimers upon ligand binding. *Cell Biochem. Biophys. 44*, 453–462.
28. Figueira, A. C. M., Neto Mde, O., Bernardes, A., Dias, S. M., Craievich, A. F., Baxter, J. D., Webb, P., and Polikarpov, I. (2007) Low-resolution structures of thyroid hormone receptor dimers and tetramers in solution. *Biochemistry 46*, 1273–1283.
29. Bollag, D. M., and Edelstein, S. T. (1991) Protein Methods, pp 143−160, Wiley Interscience, New York.
30. Lakowicz, J. R. (2002) Principles of Fluorescence Spectroscopy, 3rd ed., Springer, New York.
31. Matozo, H. C., Santos, M. A. M., Neto, M. O., Bleicher, L., Lima, L. M. T. R., Iuliano, R., Fusco, A., and Polikarpov, I. (2007) Low-resolution structure and fluorescence anisotropy analysis of protein tyrosine phosphatase η catalytic domain. *Biophys. J. 92*, 4424–4432.
32. Lima, L. M. T. R., and Silva, J. L. (2004) Positive Contribution of Hydration on DNA Binding by E2c Protein from Papillomavirus. *J. Biol. Chem. 279*, 47968–47974.
33. Cantor, C. R., and Schimmel, P. R. (1980) Biophysical Chemistry: Part III: The Behavior of Biological Macromolecules, W. H. Freeman and Company, New York.
34. Royer, C. A., and Beechem, J. M. (1992) Numerical analysis of binding data: Advantages, practical aspects, and implications. *Methods Enzymol. 210*, 481–505.
35. Royer, C. A., Smith, W. R., and Beechem, J. M. (1990) Analysis of binding in macromolecular complexes: A generalized numerical approach. *Anal. Biochem. 191*, 287–294.
36. Tilman, R., and Royer, C. A. (2008) A graphical user interface for BIOEQS: A program for simulating and analyzing complex biomolecular interactions. *Anal. Biochem. 381*, 270–272.
37. Boyer, M., Poujol, N., Margeat, E., and Royer, C. A. (2000) Quantitative characterization of the interactions between purified human estrogen receptor α and DNA using fluorescence anisotropy. *Nucleic Acids Res. 28*, 2494–2502.
38. Rastinejad, F., Evans, M., and Sigler, P. B. (1995) Structural determinants of nuclear receptor assembly on DNA direct repeats. *Nature 375*, 203–211.
39. Lu, X.-J., and Olson, W. K. (2003) 3DNA: A software package for the analysis, rebuilding and visualization of three-dimensional nucleic acid structures. *Nucleic Acids Res. 31*, 5108–5121.
40. Schwabe, J. W., Chapman, L., Finch, J. T., and Rhodes, D. (1993) The crystal structure of the estrogen receptor DNA-binding domain bound to DNA: How receptors discriminate between their response elements. *Cell 75*, 567–578.
41. Rastinejad, F., Wagner, T., Zhao, Q., and Khorasanizadeh, S. (2000) Structure of the RXR-RAR DNA-binding complex on the retinoic acid response element DR1. *EMBO J. 19*, 1045–1054.
42. Collaborative Computational Project, Number 4 (1994) The CCP4 Suite: Programs for Protein Crystallography. *Acta Crystallogr. D50*, 760–763.
43. Emsley, P., and Cowtan, K. (2004) Coot: Model-building tools for molecular graphics. *Acta Crystallogr. D60*, 2126–2132.
44. Ishimaru, D., Lima, L. M., Maia, L. F., Lopez, P. M., Ano Bom, A. P., Valente, A. P., and Silva, J. L. (2004) Reversible aggregation plays a crucial role on the folding landscape of p53 core domain. *Biophys. J. 87*, 2691–2700.
45. Abbate, E. A., Voitenleitner, C., and Botchan, M. R. (2006) Structure of the papillomavirus DNA-tethering complex E2:Brd4 and a peptide that ablates HPV chromosomal association. *Mol. Cell 24*, 877–889.
46. Lewis, H., and Gaston, K. (1999) Magnesium ions enhance the transfer of human papillomavirus E2 protein from non-specific to specific binding sites. *J. Mol. Biol. 294*, 885–896.
47. Record, M. T., Jr., Lohman, M. L., and De Haseth, P. J. (1976) Ion effects on ligand-nucleic acid interactions. *Mol. Biol. 107*, 145–158.
48. Record, M. T., Jr., deHaseth, P. L., and Lohman, T. M. (1977) Interpretation of monovalent and divalent cation effects on the lac repressor-operator interaction. *Biochemistry 16*, 4791–4796.
49. Rose, D. M., Bleam, M. L., Record, M. T., Jr., and Bryant, R. G. (1980) ^{25}Mg NMR in DNA solutions: Dominance of site binding effects. *Proc. Natl. Acad. Sci. U.S.A. 77*, 6289–6292.
50. Wyman, J., Jr. (1964) Linked functions and reciprocal effects in hemoglobin: A second look. *Adv. Protein Chem. 19*, 223–286.
51. Mengeling, B. J., Pan, F., and Privalsky, M. L. (2003) Novel mode of deoxyribonucleic acid recognition by thyroid hormone receptors: Thyroid hormone receptor β-isoforms can bind as trimers to natural response elements comprised of reiterated half-sites. *Mol. Endocrinol. 19*, 35–51.
52. Desvergne, B. (1994) How do thyroid hormone receptors bind to structurally diverse response elements? *Mol. Cell. Endocrinol. 100*, 125–131.
53. Ribeiro, R. C., Feng, W., Wagner, R. L., Costa, C. H., Pereira, A. C., Apriletti, J. W., Fletterick, R. J., and Baxter, J. D. (2001) Definition of the surface in the thyroid hormone receptor ligand binding domain for association as homodimers and heterodimers with retinoid X receptor. *J. Biol. Chem. 276*, 14987–14995.
54. Nascimento, A. S., Dias, S. M., Nunes, F. M., Aparício, R., Ambrosio, A. L., Bleicher, L., Figueira, A. C. M., Santos, M. A., de Oliveira Neto, M., Fischer, H., Togashi, M., Craievich, A. F., Garratt, R. C., Baxter, J. D., Webb, P., and Polikarpov, I. (2006) Structural rearrangements in the thyroid hormone receptor hinge domain and their putative role in the receptor function. *J. Mol. Biol. 360*, 586–598.

55. Ozers, M. S., Hill, J. J., Ervin, K., Wood, J. R., Nardulli, A. M., Royer, C. A., and Gorski, J. (1997) Equilibrium binding of estrogen receptor with DNA using fluorescence anisotropy. *J. Biol. Chem. 272*, 30405–30411.
56. Chandra, V., Huang, P., Hamuro, Y., Raghuram, S., Wang, Y., Burris, T. P., and Rastinejad, F. (2008) Structural organization of the intact PPARγ-RXRα nuclear receptor complex on DNA. *Nature 29*, 350–356.
57. Zhu, X.-G., McPhie, P., Lin, K.-H., and Cheng, S.-Y. (1996) The differential hormone-dependent transcriptional activation of thyroid hormone receptor isoforms is mediated by interplay of their domains. *J. Biol. Chem. 272*, 9048–9054.
58. Boyer, M., Poujol, N., Margeat, E., and Royer, C. (2000) Quantitative characterization of the interaction between purified human estrogen receptor α and DNA using fluorescence anisotropy. *Nucleic Acids Res. 28*, 2494–2502.
59. Mader, S., Chen, J. Y., Chen, Z., White, J., Chambon, P., and Gronemeyer, H. (1993) The patterns of binding of RAR, RXR and TR homo- and heterodimers to direct repeats are dictated by the binding specificites of the DNA binding domains. *EMBO J. 12*, 5029–5041.